

Observation of Quantized Conductance in Neutral Matter

Sebastian Krinner,¹ David Stadler,¹ Dominik Husmann,¹ Jean-Philippe Brantut,^{1,*} and Tilman Esslinger¹

¹*Department of Physics, ETH Zurich, 8093 Zurich, Switzerland*

(Dated: 20140428001600)

In transport experiments the quantum nature of matter becomes directly evident when changes in conductance occur only in discrete steps [1], with a size determined solely by Planck's constant h . The observations of quantized steps in the electric conductance [2, 3] have provided important insights into the physics of mesoscopic systems [4] and allowed for the development of quantum electronic devices [5]. Even though quantized conductance should not rely on the presence of electric charges, it has never been observed for neutral, massive particles [6]. In its most fundamental form, the phenomenon requires a quantum degenerate Fermi gas, a ballistic and adiabatic transport channel, and a constriction with dimensions comparable to the Fermi wavelength. Here we report on the observation of quantized conductance in the transport of neutral atoms. We employ high resolution lithography to shape light potentials that realize either a quantum point contact or a quantum wire for atoms. These constrictions are imprinted on a quasi two-dimensional ballistic channel connecting two adjustable reservoirs of quantum degenerate fermionic lithium atoms [7]. By tuning either a gate potential or the transverse confinement of the constrictions, we observe distinct plateaus in the conductance for atoms. The conductance in the first plateau is found to be equal to $1/h$, the universal conductance quantum. For low gate potentials we find good agreement between the experimental data and the Landauer formula, with all parameters determined a priori. Our experiment constitutes the cold atom version of a mesoscopic device and can be readily extended to more complex geometries and interacting quantum gases.

As pointed out by Landauer in 1957, conductance is the transmission of carriers from one terminal to another [8, 9]. If the carriers move adiabatically through the channel connecting the terminals, each of its transverse modes contributes with $1/h$ to the conductance

$$G = \frac{1}{h} \sum_n f(E_n - \mu), \quad (1)$$

where f is the Fermi-Dirac distribution, E_n the energy of the n -th transverse mode, and μ the chemical potential in the two terminals at equilibrium. When the temperature is sufficiently low compared to the transverse energy level

spacing, the contribution of individual modes can be isolated in a transport measurement, leading to quantized plateaus in the conductance.

Whilst ubiquitous in electronics, a two-terminal setup for atomic gases has only recently been demonstrated. Here, neutral atom currents play the role of electric currents and they are driven by a chemical potential bias rather than an electric voltage, a situation corresponding to ideal charge screening. Until now, the conductance of quasi two-dimensional multimode channels was measured, probing ballistic, diffusive and superfluid regimes [7, 10, 11]. Yet, in order to identify the contribution of an individual mode to the transport, a tightly confining channel geometry is required in which the energy separation between individual transverse modes is large compared to the temperature [12]. This requirement is also encountered in quasi one-dimensional quantum gas experiments without reservoirs [13–18].

The basis of the experiment is our transport setup [7]. In brief, a weakly interacting gas of $N = 7.5(3) \times 10^4$ fermionic ${}^6\text{Li}$ atoms is prepared in a cigar-shaped trap at a temperature of $T = 42(8) \text{ nK} = 0.11(2)T_F$, where $T_F = 385(12) \text{ nK}$ denotes the Fermi temperature. The elongated trap is then split into two reservoirs connected by a two-dimensional channel using the repulsive potential of a TEM₀₁-like mode of a laser operating at 532 nm, see Fig. 1a.

A quantum point contact (QPC) [19] is created by lithographically projecting a split gate structure onto the two-dimensional channel, see Fig. 1a and b. To do so the negative of a slit with a width of $12 \mu\text{m}$ is printed on a binary mask and illuminated with a laser beam at 532 nm. A projection system, consisting of an achromatic lens and a high numerical aperture microscope objective, demagnifies the object by a factor 11. The width of the resulting QPC in the channel region is measured to be $1.5(3) \mu\text{m}$ (FWHM) in x direction, using a second identical microscope placed opposite to the first one [20]. Since this value is comparable to the Fermi wavelength of $2.2 \mu\text{m}$ in our system, a single mode regime should be accessible. The finite width of the diffraction limited point spread function of the projection system leads to a harmonically confining potential along the x axis. The overall shape of the projected QPC potential is given by the Gaussian profile of the illuminating laser beam, whose waists are $5.6(3) \mu\text{m}$ ($33.6(6) \mu\text{m}$) along the y (x) axis in the image plane.

The QPC is characterized by its trap frequencies along z and x at its center, ν_z and ν_x , originating from the

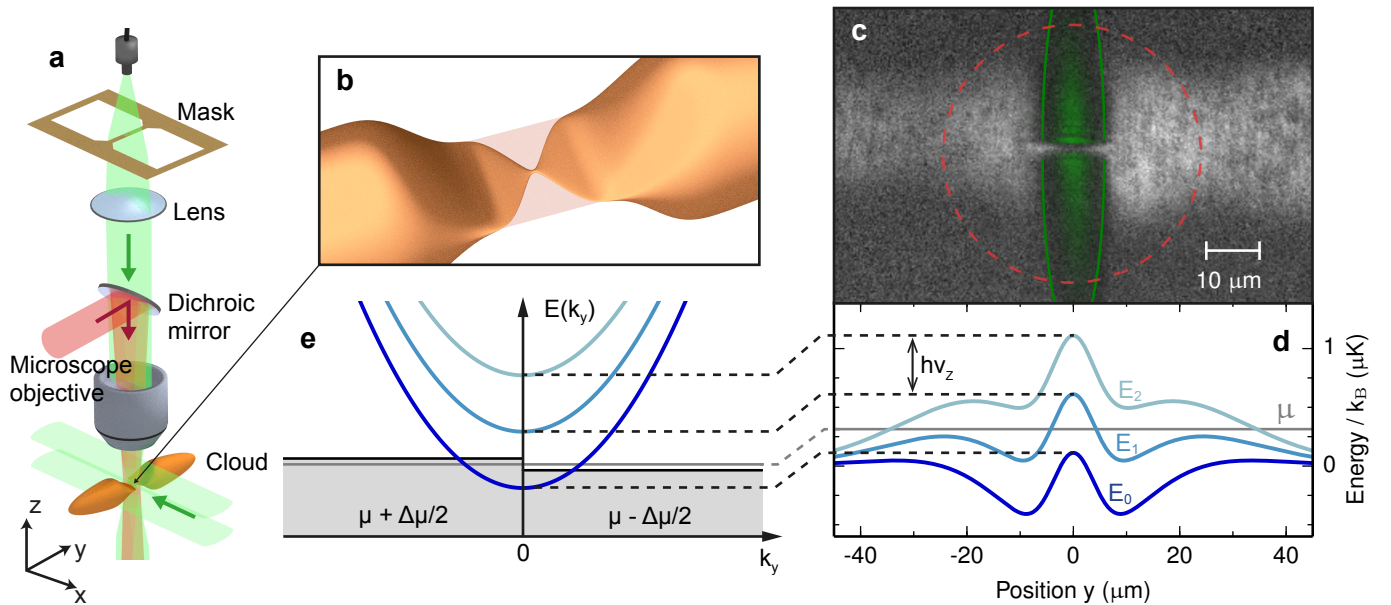


FIG. 1: **An atomic QPC.** a, Lithographic imprinting of the QPC (vertical green beam). An achromatic lens and a high numerical aperture microscope objective are used to demagnify the QPC structure onto the 2D channel region in the atomic cloud. An attractive gate potential is created by a red detuned laser beam (red beam). It is combined with the green beam on a dichroic mirror and focused onto the center of the QPC. The TEM₀₁-like laser mode creating the 2D channel is shown as a horizontal green beam propagating along the x axis. b, Zoom into the channel region: reservoirs, 2D channel and QPC are smoothly connected to each other. c, Imaged atomic density in the QPC for $\nu_z = 4.6$ kHz, $\nu_x = 29$ kHz and $V_g = 1.4$ μ K in grey scale. The overlaid elliptical green region with the horizontal cut is an image of the projected split gate structure. Green solid line and red dashed line are $1/e^2$ contours of the split gate structure and of the gate potential, respectively. d, Effective potential along the transport axis, consisting of the transverse mode energy and the gate potential (see Methods). The energy levels corresponding to the three lowest transverse modes are labeled with E_0 , E_1 and E_2 . The depicted situation corresponds to the first plateau of the $\nu_z = 10.4$ kHz data of Fig. 2. e, Energy dispersion relation of the particles in the QPC. The parabolas are offset by the quantized transverse mode energies. Left and right reservoirs are represented by grey boxes, having chemical potentials $\mu \pm \Delta\mu/2$.

harmonic confinement of the TEM₀₁-like laser beam and the lithographically imprinted constriction respectively. Typical values are $\nu_z = 10.0(4)$ kHz and $\nu_x = 30(3)$ kHz. The three lowest modes are thus separated by $h\nu_z \simeq 0.5$ μ K, which is much more than the temperature of the gas. The zero-point energy in the QPC is $E_0 = (h\nu_z + h\nu_x)/2 \simeq 1.0$ μ K, which is larger than the chemical potential $\mu = 370(11)$ nK, imposed by the reservoirs. To successively populate the transverse modes of the QPC we use an additional laser beam creating an attractive gate potential V_g at the position of the QPC, see Fig. 1c, d, e. The laser beam with a wavelength of 767 nm has a waist of 25.0(6) μ m and is propagating along the z axis.

To measure the conductance we prepare an initial particle number imbalance $\Delta N_0 = (N_L - N_R)_0 = 0.40(2)N$ between the two reservoirs, with N_L and N_R denoting the particle number in the left and right reservoir respectively. This leads to a chemical potential bias $\Delta\mu = 94(7)$ nK $\ll h\nu_z$, driving a current $I = G\Delta\mu$ across the QPC. We access the conductance by measuring the relative particle number imbalance after 1.5 s of trans-

port time, assuming linear response, and evaluating the compressibility of the reservoirs (see Methods).

Fig. 2 presents the measured conductance as a function of V_g for two different vertical confinement frequencies, $\nu_z = 10.4$ kHz and $\nu_z = 8.2$ kHz. The confinement along x is set to $\nu_x = 31.8$ kHz. Both curves start at zero conductance because the QPC is entirely closed at small gate potentials due to its zero-point energy. At the point where V_g compensates the zero-point energy the conductance starts to rise and saturates at the universal value $1/h$ as soon as the ground state mode is tuned below the chemical potential of the reservoirs. Higher modes follow accordingly upon further increase of V_g . We clearly resolve the first two conductance plateaus in the case of $\nu_z = 10.4$ kHz (open blue circles), corresponding to the population of the $(n_x = 0, n_z = 0, 1)$ modes, where n_x and n_z are the harmonic oscillator quantum numbers for the x and z direction respectively. For $\nu_z = 8.2$ kHz (filled red squares) the plateaus are narrower because the modes are more closely spaced in energy. In this case we resolve the first three modes, $(n_x = 0, n_z = 0, 1, 2)$ and even the onset of the $(0, 3)$ mode is visible.

The inset of Fig. 2 shows a zoom on the first conductance plateau. When substituting V_g by the total energy $E_{\text{tot}} = V_g + \mu$ of the particles minus E_0 and normalizing to $h\nu_z$, both data sets fall on top of each other as a consequence of universality, with the width of the plateau given by one unit of $h\nu_z$. The absolute accuracy of our conductance measurement is limited by the uncertainty in the compressibility of the reservoirs, which amounts to 11% (see Methods).

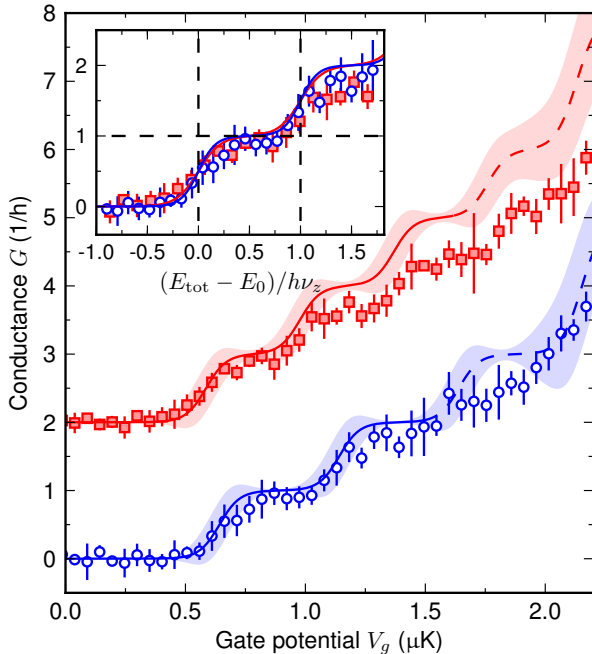


FIG. 2: **Conductance as a function of gate potential.** Open blue circles correspond to a vertical confinement of $\nu_z = 10.4$ kHz. Filled red squares correspond to $\nu_z = 8.2$ kHz and are vertically shifted by two units for clarity. Each data point represents the mean of six measurements and error bars indicate one standard deviation. Solid lines are theoretical predictions based on the Landauer formula of conductance. The shaded regions reflect the uncertainties in the input parameters (see text). Dashed lines are continuations of the solid lines and correspond to a change in the effective potential (see Methods). Inset: first conductance plateau as a function of reduced energy, showing universal scaling. Vertical dashed lines indicate the width of the first plateau, whereas the horizontal dashed line indicates the universal conductance value $1/h$.

The quantization of conductance is universal and should not depend on the control parameter. To demonstrate this, we next use the horizontal confinement ν_x of the QPC as a tuning parameter and keep the gate potential fixed. This is the counterpart of the celebrated measurement in solid state physics, where the split gate voltage is tuned to reveal quantized conductance [2, 3]. The blue data points in Fig. 3 present this measurement for $\nu_z = 10.9$ kHz and $V_g = 1.0(1)$ μK . We identify three increasingly wider plateaus centered

at $\nu_x = 12, 20, 35$ kHz. They correspond to the successive closing of the (1,0), (0,1) and (0,0) mode. The red data points in Fig. 3 correspond to $\nu_z = 9.2$ kHz and $V_g = 0.8(1)$ μK and show the same features as the blue data, with a reduced plateau width due to a smaller ν_z .

We compare our data to theoretical predictions (solid lines in Fig. 2 and 3) of the Landauer formula in the limit of entirely adiabatic and ballistic transport, Eqn. (1), without any fit parameter (see Methods). The input parameters T , μ , $\Delta\mu$, ν_x , ν_z , V_g are all independently measured quantities. Positions and widths of the plateaus are overall well predicted. The conductances on the plateaus reach the universal values for moderate gate potentials. For larger gate potentials (see Fig. 2) the conductance is reduced with respect to the prediction. A possible reason is a small non-adiabaticity in the motion of the particles introduced by the gate potential, which accelerates the particles more and more towards the QPC as its strength is increased.

The sharpness of the transition from one plateau to the next is set by the finite temperature. We checked numerically within the adiabatic approximation that broadening due to tunneling below the barrier or reflections above it [21] is much smaller than the relevant thermal broadening of the Fermi edge of $\sim 4k_B T$ [5]. Further, we do not observe any non-linear effects [22] due to the applied finite bias $\Delta\mu$ because it is smaller than $\sim 4k_B T$, too.

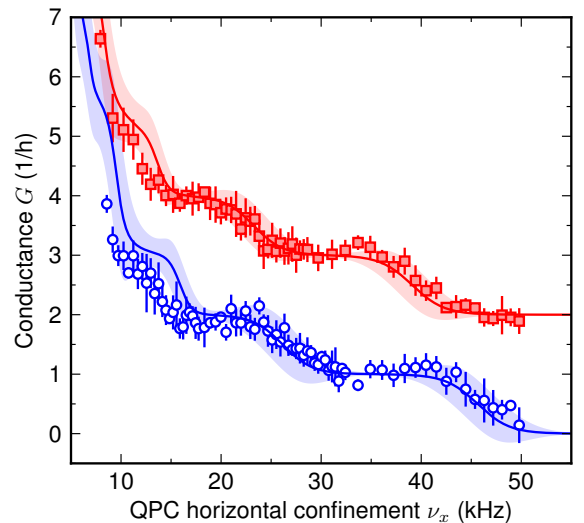


FIG. 3: **Conductance as a function of horizontal confinement.** Open blue circles correspond to a vertical confinement of $\nu_z = 10.9$ kHz and a gate potential of $V_g = 1.0(1)$ μK . Filled red squares correspond to $\nu_z = 9.2$ kHz and $V_g = 0.8(1)$ μK , and are vertically shifted by two units for clarity. Solid lines are theoretical predictions based on the Landauer formula of conductance. The shaded regions reflect the uncertainties in the input parameters (see text). Error bars are the same as in Fig. 2.

The chemical potential or voltage in a ballistic con-

striction drops at its contacts [23], leading to universal conductance values independent of the length of the constriction. We demonstrate this by creating a long quantum wire (QW), see inset of Fig. 4. It has a length of $19.0(6) \mu\text{m}$ and the same width of $1.5(3) \mu\text{m}$ as the QPC. The projected structure is spatially smoothed by the low-pass filtering of the projection system. The triangular-shaped openings further smoothen the transition from the QW to the 2D channel to avoid reflections at the openings [24, 25]. The resulting effective potential, with the openings modeled by an error function, is shown in the inset of Fig. 4. It is highest at the entrance and exit of the QW, which is a consequence of the nearly uniform confinement in combination with the Gaussian envelope of the attractive gate beam. The detection of single quanta of conductance is found to be less robust in this configuration, most likely because the points of highest potential are located at a slope of the gate beam. Nevertheless quantized conductance plateaus are observed for tight confinement ($\nu_x = 24.6 \text{ kHz}$, $\nu_z = 8.7 \text{ kHz}$, black circles in Fig. 4), using the gate potential as a tuning parameter. They are well reproduced by theory, up to a 10-20% reduction in height for the second and third plateau. Possible interference effects, such as above-barrier resonances [24] are not observed, likely because the finite temperature leads to a coherence length of the atoms of $7(1) \mu\text{m}$, which is shorter than the length of the QW.

The green data in Fig. 4 demonstrate how the plateaus disappear when ν_z is lowered to 5.5 kHz . The conductance starts to rise at a lower gate potential because of the reduced zero-point energy. Well defined plateaus are no longer visible due to the reduced ratio of $h\nu_z$ to temperature. However we observe a change in slope of conductance by a factor of ~ 2 at $V_g \simeq 1.75 \mu\text{K}$, which is due to the entrance of the first excited state along the x direction. More precisely, when V_g is increased from 0.25 to $1.75 \mu\text{K}$ the states ($n_x = 0, n_z = 0, 1, 2, 3$) enter, whereas above $V_g = 1.75 \mu\text{K}$ the states ($n_x = 0, n_z = 4, 5, \dots$) and the states ($n_x = 1, n_z = 0, 1, \dots$) enter, giving rise to a change in slope by a factor of 2. This feature is well covered by theory.

The demonstrated projection technique in combination with the ability to control all microscopic parameters a priori paves the way towards the quantum simulation of complex devices based on strongly correlated quantum gases. The detection of conductance at the level of single quanta provides access to the physics of topological edge states [26], transport in the vicinity of a quantum phase transition [27], and universal conductance fluctuations [28].

We acknowledge fruitful discussions with G. Blatter, K. Ensslin, C. Glattli, T. Giamarchi, C. Grenier and M. Lebrat, and thank C. Chin, T. Ihn, Y. Imry, and W. Zwerger for their careful reading of the manuscript and discussions. We acknowledge financing from NCCR QSIT, the ERC Project SQMS, the FP7 project SIQS,

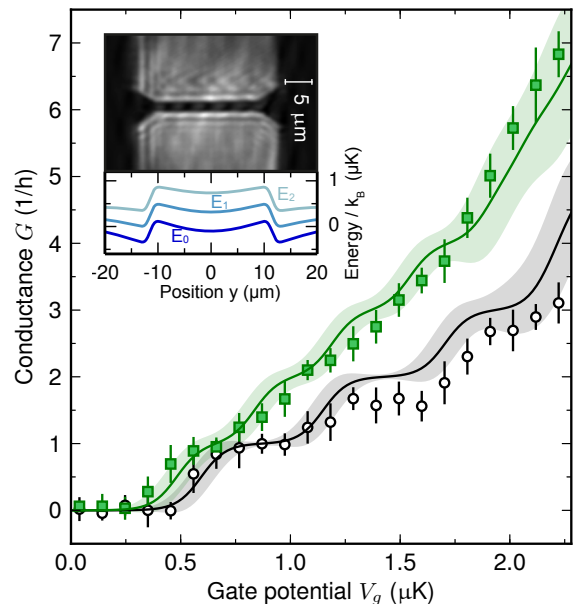


FIG. 4: **Quantum wire: conductance as a function of gate potential.** Open black circles correspond to a vertical confinement of $\nu_z = 8.7 \text{ kHz}$, and filled green squares to a lower confinement of $\nu_z = 5.5 \text{ kHz}$. For the stronger confinement clear conductance plateaus are observed. The weaker confinement illustrates the entrance of the first excited mode along the x direction (see text). Solid lines are theoretical predictions based on the Landauer formula of conductance. Shaded regions and error bars are the same as in Fig. 2. The inset shows the lithographically imprinted wire as imaged by a second identical microscope objective. Below it, the corresponding effective potentials are drawn for the three lowest transverse modes, E_0 , E_1 , E_2 , for the parameters at the first plateau of the $\nu_z = 8.7 \text{ kHz}$ data.

and ETHZ. J.P.B. is supported by the Ambizione program of SNF.

METHODS SUMMARY

A weakly interacting degenerate Fermi gas of ${}^6\text{Li}$ atoms is prepared in a balanced spin mixture of the lowest and third lowest hyperfine states in a hybrid magnetic and optical dipole trap at a homogenous magnetic field of 552 G , where the scattering length is $-100a_0$ with a_0 denoting Bohr's radius. To create a particle number imbalance between the two reservoirs we shift the trapping potential with respect to the QPC/QW along the y axis during evaporative cooling. Shifting the trap back while blocking the transport with an additional repulsive gate laser beam [29] results in a chemical potential bias. The transport process is started by removing the repulsive gate beam. After a transport time of 1.5 s we switch it back on and measure the atom number in each reservoir. The temporal evolution of $\Delta N/N$ follows an exponen-

tial decay with a time constant $\tau = 2G/C$, where C is the compressibility of a single reservoir. We infer τ from the knowledge of the initial imbalance and the imbalance after 1.5 s of transport time. Evaluating C by assuming a non-interacting Fermi gas in a half-harmonic trap [29] and taking into account the two-dimensional channel, directly yields G . All quantities in the text are stated for a single hyperfine state, implying that the conductance plateaus appear in multiples of $1/h$ and not $2/h$. The transverse trapping frequencies of the QPC and QW are measured by parametric heating. The theory curves for the conductance rely on the adiabatic approximation [5, 21], allowing for a separation of longitudinal (y) and transverse (x, z) variables. In the resulting one-dimensional Schrödinger equation the transverse energy $E_n(y) = E_{n_x, n_z}(y)$ and the gate potential $V_g(y)$ form the effective potential drawn in Fig. 1d and in the inset of Fig. 4.

METHODS

Experimental Setup

Our experiment uses the system described in [7, 29]. In brief, a degenerate Fermi gas of ${}^6\text{Li}$ atoms is produced by evaporative cooling of a balanced spin mixture of the lowest and third lowest hyperfine states in a hybrid magnetic and optical dipole trap at a homogenous magnetic field of 388 G, using a magnetic field gradient [30]. The dipole trap operates at a wavelength of 1064 nm, has a waist of $70\ \mu\text{m}$ and a trap depth of $1.2\ \mu\text{K}$. The experiments are performed in a homogeneous magnetic field of 552 G, where the scattering length is $-100\ a_0$, a_0 denoting Bohr's radius. This allows for sufficiently fast thermalization of the reservoirs, while at the same time ensuring a ballistic transport channel. All quantities in the text are stated for a single hyperfine state, implying that the conductance plateaus appear in multiples of $1/h$ and not $2/h$.

Transport Sequence

During the preparation of the degenerate gas, a magnetic field gradient of $0.2\ \text{mT/m}$ is applied along the y axis in order to shift the trap with respect to the QPC. A repulsive elliptic gate beam focused onto the center of the QPC is used to separate the two reservoirs as in [29]. The power of the laser beams creating the two-dimensional channel is ramped from zero to its final value within 200 ms. The same ramp is applied to the laser beam creating the QPC. Then, evaporative cooling is enforced by using a magnetic field gradient along the z axis [30]. This procedure results in a well defined particle number imbalance between the two reservoirs. Next, the dipole

trap is adiabatically decompressed from a trap depth of $5.6\ \mu\text{K}$ to a final depth of $1.2\ \mu\text{K}$ within 200 ms to further reduce the absolute temperature of the gas. During the same time interval the attractive gate potential is ramped from zero to V_g . Finally, the magnetic field gradient along y is ramped to zero within 60 ms, resulting in a well-defined chemical potential difference $\Delta\mu$ between the two reservoirs. We start the transport process by removing the repulsive gate beam. After a transport time of 1.5 s we switch back on the repulsive gate beam to stop the transport process and we measure the atom number in both reservoirs via absorption imaging.

Conductance Evaluation

From the equation for the current, $I = G\Delta\mu$, we obtain that the temporal evolution of the particle number imbalance between left and right reservoirs, $\Delta N = N_L - N_R$, is governed in linear response by the equation

$$\frac{d}{dt}(\Delta N/N) = -\frac{G}{C_{\text{eff}}}(\Delta N/N), \quad (2)$$

where $N = N_L + N_R$ is the total atom number and $C_{\text{eff}} = (1/C_L + 1/C_R)^{-1}$ is an effective compressibility determined by the compressibilities of the single reservoirs at equilibrium. In agreement with this equation we observe an exponential decay of the relative particle number imbalance as a function of time, the time constant being $\tau = C_{\text{eff}}/G$. We evaluate G by measuring τ and evaluating C_{eff} . The error made when substituting $\Delta\mu$ by $\Delta N/C_{\text{eff}}$ to obtain the linear response Eqn. 2 is smaller than 5% at the largest value of $\Delta N/N = 0.4$.

τ is determined by measuring the relative particle number imbalance at $t = 0$ and after a transport time of $t_{\text{tr}} = 1.5\ \text{s}$. From the solution of Eqn. (2) we obtain

$$\frac{1}{\tau} = \frac{1}{t_{\text{tr}}}\log\left(\frac{\Delta N}{N}(t=0)\right) - \frac{1}{t_{\text{tr}}}\log\left(\frac{\Delta N}{N}(t=t_{\text{tr}})\right), \quad (3)$$

where a constant offset of $-0.20(1)$ is subtracted from both imbalances. This offset originates partly from the relative alignment of the gate beam and the lithographic system, and for the data of Fig. 2 it varied linearly from -0.20 to -0.16 over the shown range.

The compressibilities $C_L = C_R = C$ of the identical reservoirs are calculated from the trap geometry, particle number and temperature, assuming a non-interacting Fermi gas. In brief, the trapping potential is harmonic along the x and z direction and half-harmonic along the y direction [29] with trapping frequencies of (194, 23.5, 157) Hz along the x, y and z direction. The effect of the repulsive potential of the TEM_{01} -like laser mode, creating the two-dimensional channel, is to shift the chemical potential by 17% towards larger values with respect to the unperturbed cloud. The compressibility is

almost not affected. The systematic uncertainty in C_{eff} amounts to 11%, which is due to the calibration error in the total particle number and an uncertainty in the overall trapping potential.

Trapping Frequencies of the QPC/QW

The transverse trapping frequencies of the QPC and QW, ν_x and ν_z , are measured by parametric heating in a dipole trap created by a laser beam with a waist of $8\ \mu\text{m}$ and a wavelength of $767\ \text{nm}$, propagating along the z axis. The observed resonances have relative widths (FWHM) of $\delta\nu_z/\nu_z = 0.05$ and $\delta\nu_x/\nu_x = 0.30(5)$. ν_z is found to depend weakly on ν_x . This is because the darkness of the projected QPC structure decreases due to diffraction when moving out of focus along the z axis, thus creating an additional confinement along z . We measure this contribution to be $\tilde{\nu}_z = 0.16\nu_x$. Hence ν_z is given by $\nu_z = \sqrt{\nu_{z,0}^2 + (0.16\nu_x)^2}$, where $\nu_{z,0}$ is the trapping frequency in the absence of the QPC. The values of ν_z stated in the text for the data of Fig. 3 are evaluated for $\nu_x = 31.8\ \text{kHz}$ in order to be comparable to the values set for the data of Fig. 2. For the shown range of $\nu_x \in [10, 50]\ \text{kHz}$, ν_z varies by 12% (16%) around its mean value for the $\nu_z = 10.9\ \text{kHz}$ (9.2 kHz) data.

Adiabatic Approximation and Theory Curves

The computation of the conductance makes use of the adiabatic approximation [5, 21], allowing for a separation of longitudinal (y) and transverse (x, z) variables. It neglects scattering between different transverse modes and is justified if the confinement of the constriction varies smoothly along the transport direction. This is to a good approximation the case for both the QPC with its gaussian envelope and the QW with its triangular-shaped openings that are smoothed by the inherent low-pass filtering of the projection system. In the resulting one-dimensional Schrödinger equation the transverse energy $E_n(y) = E_{n_x, n_z}(y) = \hbar\nu_x f_x(y)(n_x + 1/2) + \hbar\nu_z f_z(y)(n_z + 1/2)$, with $f_{x,z}(y)$ describing the spatial variation of the trapping frequencies, acts as an additional potential. Together with the gate potential $V_g(y)$ it forms the effective potential drawn in Fig. 1d and in the inset of Fig. 4. For the QPC we have $f_{x,z}(y) = \exp(-y^2/w_{x,z}^2)$, with $w_x = 5.6(3)\ \mu\text{m}$ and $w_z = 30(1)\ \mu\text{m}$, whereas for the QW f_x is constant along the wire, with its edges modeled by an error function.

The theory lines in Fig. 2 are dashed above $V_g \sim 1.5\ \mu\text{K}$ because at this point the maximum of the effective potential moves from the center to the sides of the QPC, which is not taken into account in the theory. This effect is not expected to explain the observed shift of the

conductance below the universal values for large gate potentials.

The conductance is calculated from Eqn. 1, which we obtain from the two-terminal Landauer formula in the adiabatic regime [5]

$$G = \frac{1}{h} \sum_n \int_{-\infty}^{\infty} dE T_n(E) \left(-\frac{\partial f}{\partial E}(E - \mu) \right) \quad (4)$$

by setting the transmission probability $T_n(E) = \Theta(E - E_n)$, with $\Theta(E - E_n)$ the Heaviside step function. This substitution corresponds to the semiclassical approximation, where the transmission probability for particles is one if their total energy is larger than their transverse energy and zero otherwise. It neglects tunneling below the barrier and reflections above it [21], which would lead to a broadening of $T_n(E)$. We checked numerically that for our geometry this broadening is much smaller than the thermal broadening of the Fermi-Dirac distribution and can thus be neglected.

Taking into account the gate potential for the conductance evaluation, Eqn. 1 reads:

$$G = \frac{1}{h} \sum_n f \left(\frac{E_n - V_g - \mu}{k_B T} \right). \quad (5)$$

In the case of the quantum wire V_g is multiplied by a factor $\exp(-9.5^2/25^2)$ to account for the fact that the points of largest effective potential are located $9.5\ \mu\text{m}$ from the center of gate potential and QW. The shaded error regions cover statistical and systematic errors of the input parameters and are determined using gaussian error propagation. The main contribution in Fig. 2 and 4 is the uncertainty in ν_x , whereas in Fig. 3 it is V_g .

* Electronic address: brantutj@phys.ethz.ch

- [1] Imry, Y. *Physics of mesoscopic systems*, in *Directions in Condensed Matter*, edited by G. Grinstein, G. Mazenko (Singapore, World Scientific, 1986).
- [2] van Wees, B. J. *et al.* Quantized conductance of point contacts in a two-dimensional electron gas. *Phys. Rev. Lett.* **60**, 848–850 (1988).
- [3] Wharam, D. A. *et al.* One-dimensional transport and the quantisation of the ballistic resistance. *J. Phys. C: Solid State Phys.* **21**, L209 (1988).
- [4] Imry, Y. *Introduction to Mesoscopic Physics* (Oxford University Press, 2002).
- [5] Ihn, T. *Semiconductor Nanostructures* (Oxford University Press, 2010).
- [6] Sato, Y., Eom, B.-H. & Packard, R. On the feasibility of detecting quantized conductance in neutral matter. *J Low Temp Phys* **141**, 99–109 (2005).
- [7] Brantut, J.-P., Meineke, J., Stadler, D., Krinner, S. & Esslinger, T. Conduction of ultracold fermions through a mesoscopic channel. *Science* **337**, 1069–1071 (2012).

- [8] Landauer, R. Spatial variation of currents and fields due to localized scatterers in metallic conduction. *IBM Journal of Research and Development* **1**, 223–231 (1957).
- [9] Büttiker, M., Imry, Y., Landauer, R. & Pinhas, S. Generalized many-channel conductance formula with application to small rings. *Phys. Rev. B* **31**, 6207–6215 (1985).
- [10] Stadler, D., Krinner, S., Meineke, J., Brantut, J.-P. & Esslinger, T. Observing the drop of resistance in the flow of a superfluid fermi gas. *Nature* **491**, 736–739 (2012).
- [11] Krinner, S., Stadler, D., Meineke, J., Brantut, J.-P. & Esslinger, T. Superfluidity with disorder in a thin film of quantum gas. *Phys. Rev. Lett.* **110**, 100601 (2013).
- [12] Thywissen, J. H., Westervelt, R. M. & Prentiss, M. Quantum point contacts for neutral atoms. *Phys. Rev. Lett.* **83**, 3762–3765 (1999).
- [13] Görlitz, A. *et al.* Realization of bose-einstein condensates in lower dimensions. *Phys. Rev. Lett.* **87**, 130402 (2001).
- [14] Moritz, H., Stöferle, T., Köhl, M. & Esslinger, T. Exciting collective oscillations in a trapped 1D gas. *Phys. Rev. Lett.* **91**, 250402 (2003).
- [15] Paredes, B. *et al.* Tonks-girardeau gas of ultracold atoms in an optical lattice. *Nature* **429**, 277–281 (2004).
- [16] Kinoshita, T., Wenger, T. & Weiss, D. S. Observation of a one-dimensional tonks-girardeau gas. *Science* **305**, 1125–1128 (2004).
- [17] Bouchoule, I., van Druten, N. & Westbrook, C. *Atom Chips and One-Dimensional Bose Gases*, in *Atom Chips*, edited by J. Reichel, V. Vuletic (John Wiley & Sons, 2010).
- [18] Serwane, F. *et al.* Deterministic preparation of a tunable few-fermion system. *Science* **332**, 336–338 (2011).
- [19] Houten, H. v. & Beenakker, C. Quantum point contacts. *Physics Today* **49**, 22–27 (1996).
- [20] Zimmermann, B., Müller, T., Meineke, J., Esslinger, T. & Moritz, H. High-resolution imaging of ultracold fermions in microscopically tailored optical potentials. *New Journal of Physics* **13**, 043007 (2011).
- [21] Glazman, L. I., Lesovik, G. B., Khmel’Nitskiĭ, D. E. & Shekhter, R. I. Reflectionless quantum transport and fundamental ballistic-resistance steps in microscopic constrictions. *Soviet Journal of Experimental and Theoretical Physics Letters* **48**, 238 (1988).
- [22] Kouwenhoven, L. P. *et al.* Nonlinear conductance of quantum point contacts. *Phys. Rev. B* **39**, 8040–8043 (1989).
- [23] Ulreich, S. & Zwerger, W. Where is the potential drop in a quantum point contact? *Superlattices and Microstructures* **23**, 719–730 (1998).
- [24] Szafer, A. & Stone, A. D. Theory of quantum conduction through a constriction. *Phys. Rev. Lett.* **62**, 300–303 (1989).
- [25] Yacoby, A. & Imry, Y. Quantization of the conductance of ballistic point contacts beyond the adiabatic approximation. *Phys. Rev. B* **41**, 5341–5350 (1990).
- [26] Hasan, M. Z. & Kane, C. L. Colloquium: Topological insulators. *Rev. Mod. Phys.* **82**, 3045–3067 (2010).
- [27] Sachdev, S. *Quantum Phase Transitions* (Cambridge University Press, 2011).
- [28] Lee, P. A. & Stone, A. D. Universal conductance fluctuations in metals. *Phys. Rev. Lett.* **55** (1985).
- [29] Brantut, J.-P. *et al.* A thermoelectric heat engine with ultracold atoms. *Science* **342**, 713–715 (2013).
- [30] Hung, C.-L., Zhang, X., Gemelke, N. & Chin, C. Accelerating evaporative cooling of atoms into bose-einstein condensation in optical traps. *Phys. Rev. A* **78**, 011604 (2008).